Inorg. Chem. **2007**, *46*, 1966–1974

Localization or Delocalization in the Electronic Structure of Creutz–Taube-Type Complexes in Aqueous Solution

Daisuke Yokogawa,[†] Hirofumi Sato,*[,†] Yoshihide Nakao,[†] and Shigeyoshi Sakaki*[,†,‡]

Department of Molecular Engineering, Graduate School of Engineering, Kyoto University, Nishikyo-ku, Kyoto 615-8510, Japan, and Fukui Institute for Fundamental Chemistry, Kyoto University, Takano-Nishihiraki-cho 34-4, Sakyo-ku, Kyoto 606-8103, Japan

Received January 31, 2006

Creutz–Taube complex, $[(NH_3)_5Ru–pyrazine–Ru(NH_3)_5]^{5+}$ (**1**), and its analogues, $[(NH_3)_5Os–pyrazine–Os(NH_3)_5]^{5+}$ (**2**), $[(NH_3)_5Ru(4,4'\text{-bipyridine})Ru(NH_3)_5]^{5+}$ (**3**), and $[(NH_3)_5Os(4,4'\text{-bipyridine})Os(NH_3)_5]^{5+}$ (**4**), were theoretically investigated by the combination of a two-state model and the dielectric continuum model. Their electronic structures are very sensitive to the metal, ligand, and solvent. In the gas phase, the electronic structures of **1**–**4** would be completely delocalized. In aqueous solution, that of **3** becomes localized because the polar solvent stabilizes the localized electronic structure with the large dipole moment. However, **1** and **2** are still delocalized in aqueous solution. In **4**, the electronic structure would be localized when the dihedral angle between two pyridyl rings is 80°, while it would become delocalized when the angle is small. The origins of the difference are the smaller overlap integral and larger energy difference between two diabatic states, of which electronic structure is almost localized on each metal center.

Introduction

Mixed-valence complexes containing several metal centers with different oxidation states have received intense theoretical and experimental interests because of their flexible electronic structures and potential ability in molecular electronics.[1] Their electronic structures are explained in terms of a superposition of two localized electronic structures. Robin and Day classified mixed-valence complexes into three classes, namely, classes I, II, and III, considering the strength of the metal−metal interaction, which determines the magnitude of mixing of the two localized, electronic structures. In class I, the metal−metal interaction is negligibly weak, and the distribution of the excess electron or the hole is completely localized upon one of the metal centers. In class III, the interaction is strong enough, and the distribution is fully delocalized. The interaction in class II is intermediate between them. This classification of the mixed-valence complexes is discussed in many theoretical calculations and in such experimental measurements as intervalence charge-transfer spectra (IVCT).[1−4] Both experimental and theoretical works for mixed-valence complexes were summarized in detail by Demadis et al.[5] Recently, Reimers et al. discussed electronic structure and some physical properties using reorganization energy.[6]

Creutz−Taube complex, $[(NH_3)_5Ru-pyrazine-Ru(NH_3)_5]^{5+}$ (**1** in Figure 1),[7,8] is one of the typical mixed-valence complexes. There has been heated controversy over how much its electronic structure is localized. In this regard, many experimental and theoretical investigations have been performed so far in order to understand the electronic structure. For instance, the electronic structure was investigated by the Stark effect,[9] near-IR−vis spectra,[10] and IVCT spectra.[2] Creutz discussed the relationship between the physical

* To whom correspondence should be addressed. E-mail: sakaki@moleng.kyoto-u.ac.jp.
[†] Graduate School of Engineering.
[‡] Fukui Institute for Fundamental Chemistry.

(1) Braun-Sand, S. B.; Wiest, O. *J. Phys. Chem. A* **2003**, *107*, 285−291.
(2) Fürholz, U.; Bürgi, H.-B.; Wagner, F. E.; Stebler, A.; Ammeter, J. H.; Krausz, E.; Clark, R. J. H.; Stead, M. J.; Ludi, A. *J. Am. Chem. Soc.* **1984**, *106*, 121−123.
(3) Creutz, C. *Inorg. Chem.* **1978**, *17*, 3723−3725.
(4) Sutton, J. E.; Sutton, P. M.; Taube, H. *Inorg. Chem.* **1979**, *18*, 1017−1021.
(5) Demadis, K. D.; Hartshorn, C. M.; Meyer, T. J. *Chem. Rev.* **2001**, *101*, 2655−2685.
(6) Reimers, J. R.; Cai, Z.-L.; Hush, N. S. *Chem. Phys.* **2005**, *319*, 39−51.
(7) Creutz, C.; Taube, H. *J. Am. Chem. Soc.* **1973**, *95*, 1086−1094.
(8) Creutz, C. *Prog. Inorg. Chem.* **1983**, *30*, 1−73.
(9) Oh, D. H.; Sano, M.; Boxer, S. G. *J. Am. Chem. Soc.* **1991**, *113*, 6880−6890.
(10) Oh, D. H.; Boxer, S. G. *J. Am. Chem. Soc.* **1990**, *112*, 8161−8162.

10.1021/ic060173a CCC: $37.00
Published on Web 02/14/2007

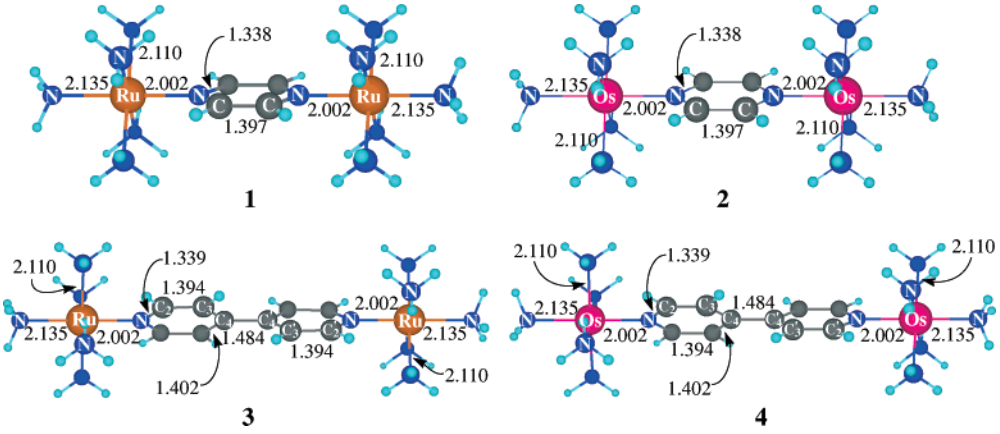

Figure 1. Geometries of $[(NH_3)_5Ru-pyrazine-Ru(NH_3)_5]^{5+}$ (**1**), $[(NH_3)_5Os-pyrazine-Os(NH_3)_5]^{5+}$ (**2**), $[(NH_3)_5Ru(4,4'\text{-bipyridine})Ru(NH_3)_5]^{5+}$ (**3**), and $[(NH_3)_5Os(4,4'\text{-bipyridine})Os(NH_3)_5]^{5+}$ (**4**) used in this work (unit, Å).

properties of these complexes and the mechanisms of electron-transfer processes in her recent review of d^6-d^5 iron, ruthenium, and osmium complexes and showed that the Creutz−Taube complex is delocalized, while the larger bipyridine-bridged complex is localized in aqueous solution.[8] Density functional theory (DFT),[1,11−13] MP2,[13] and complete active-space SCF (CASSCF) calculations[14] were performed as well. All of these studies indicated that the electronic structure is delocalized in this complex due to its strong metal−metal interaction; in other words, this complex belongs to class III.

On the other hand, the electronic structure of the 4,4′-bipyridine-bridged dinuclear Ru complex, $[(NH_3)_5Ru(4,4'\text{-bipyridine})Ru(NH_3)_5]^{5+}$ (**3** in Figure 1), was reported to be quite different from that of **1**. The Stark effect[9] and IVCT spectra[3,4] indicated that the metal−metal interaction of **3** is weak and that the electronic structure is substantially localized. Ferreti et al.[15] explained this electronic structure and visible spectra by using a four-site vibronic model. Marcus−Hush theory was also applied to evaluate the IVCT spectra of **3**.[16−19] Besides these studies, only a few computational studies of **3** have been reported, to our knowledge, in which DFT,[1] CNDO/S,[14] and CI methods[20] have been used. In these previous studies, solvation effects were not taken into consideration, except for one pioneering work[20] in which the continuum model was employed to incorporate solvent effect. In reality, however, solvation effects should be taken into consideration because the localized electronic structure is significantly stabilized by polar solvent. Another important issue is to consider its multireference nature in the electronic structure, which is closely related to mixing of localized wave functions. Standard methods such as CASSCF might not be applicable to these mixed-valence complexes in reasonable computing time because of their large sizes; see **3** for an example.

In the present article, we theoretically investigated **1**, **3**, the pyrazine-bridged dinuclear Os complex, $[(NH_3)_5Os-pyrazine-Os(NH_3)_5]^{5+}$ (**2** in Figure 1), and the 4,4′-bipyridine-bridged dinuclear Os complex, $[(NH_3)_5Os(4,4'\text{-bipyridine})Os(NH_3)_5]^{5+}$ (**4** in Figure 1). To our knowledge, complexes **2** and **4** are not known experimentally. In fact, to understand the true nature of the mixed-valence complexes, the consideration of the vibration coupling and the time scale of solvation is indispensable, as reviewed recently. However, it is also important to theoretically evaluate the electronic structure of real molecules of mixed-valence complexes with the static solvation effect. In this work, we evaluated some factors which determine the localization/delocalization of the ions without modeling and tried to relate them with fundamental parameters such as overlap and energy gap. Though our study does not incorporate vibration coupling and solvation time scale,[5] we believe the knowledge of the relation between fundamental parameters and the localization/delocalization nature is also worthwhile to understand these mixed-valence complexes.

Method and Computations

Method. As described in the preceding section, the metal−metal coupling in **1** is considered very strong, and that of **3** is considered very weak. The DFT method can be applied to the complexes with a strong metal−metal interaction, but it seems to be difficult to apply to the mixed-valence complexes with a weak metal−metal interaction because the DFT method tends to overestimate delocalized character.[13] CASSCF and CASPT2 methods are believed to be the most reliable for this type of compound. However, it is noted also that the mixed-valence complexes are too large to apply the CASSCF method.

In the present work, we employed a method proposed by Farazdel et al.[21] to treat the multireference nature of the wave function. The

(11) Bencini, A.; Ciofini, I.; Daul, C. A.; Ferretti, A. *J. Am. Chem. Soc.* **1999**, *121*, 11418−11424.
(12) Chen, Z.; Bian, J.; Zhang, L.; Li, S. *J. Chem. Phys.* **1999**, *111*, 10926−10933.
(13) Hardesty, J.; Goh, S. K.; Marynick, D. S. *J. Mol. Struct: THEOCHEM* **2002**, *588*, 223−226.
(14) Broo, A.; Larsson, S. *Chem. Phys.* **1992**, *161*, 363−378.
(15) Ferretti, A.; Improta, R.; Lami, A.; Villani, G. *J. Phys. Chem. A* **2000**, *104*, 9591−9599.
(16) Allen, G. C.; Hush, N. S. *Prog. Inorg. Chem.* **1967**, *8*, 357−389.
(17) Hush, N. S. *Prog. Inorg. Chem.* **1967**, *8*, 391−444.
(18) Hupp, J. T.; Dong, Y.; Blackbourn, R. L.; Lu, H. *J. Phys. Chem.* **1993**, *97*, 3278−3282.
(19) Lau, K. W.; Hu, A. M.-H.; Yen, M. H.-J.; Fung, E. Y.; Grzybicki, S.; Matamoros, R.; Curtis, J. C. *Inorg. Chem. Acta* **1994**, *226*, 137−143.
(20) Cacelli, I.; Ferretti, A.; Toniolo, A. *J. Phys. Chem. A* **2001**, *105*, 4480−4487.
(21) Farazdel, A.; Dupuis, M.; Clementi, E.; Aviram, A. *J. Am. Chem. Soc.* **1990**, *112*, 4206−4214.

first step of this method is to calculate two wave functions, Ψ_A and Ψ_B, by the UHF method with the same geometry, where symmetry-broken UHF orbitals are employed.[22] In Ψ_A, the excess electron is localized on one metal center, while in Ψ_B, it is localized on the other metal center. These Ψ_A and Ψ_B correspond to the nonorthogonal diabatic states.[23] The second step is to construct adiabatic wave functions, Ψ_{E+} and Ψ_{E-}, from Ψ_A and Ψ_B, as follows

$$\Psi_{E+/-} = C_A\Psi_A + C_B\Psi_B \tag{1}$$

Coefficients and the energies $E_{+/-}$ of the adiabatic states can be obtained by solving the following secular equation

$$\begin{vmatrix} H_{AA} - E & H_{AB} - ES_{AB} \\ H_{AB} - ES_{AB} & H_{BB} - E \end{vmatrix} = 0 \tag{2}$$

where $H_{AA} = \langle\Psi_A|H|\Psi_A\rangle$, $H_{BB} = \langle\Psi_B|H|\Psi_B\rangle$, $H_{AB} = \langle\Psi_A|H|\Psi_B\rangle$, and $S_{AB} = \langle\Psi_A|\Psi_B\rangle$.

The solvation effects were evaluated by considering the interaction of the point charge and the dipole moment of the solute with the reaction field, in which the solute was placed in a spherical cavity immersed in a continuous medium with a dielectric constant ϵ. In this situation, the solvation free-energy change, ΔG, is given by eq 3

$$\Delta G = -\frac{\epsilon - 1}{2\epsilon}\frac{q^2}{a} - \frac{\epsilon - 1}{2\epsilon + 1}\frac{\mu^2}{a^3} \tag{3}$$

where q is the total charge, μ is the dipole moment, and a is a radius of the spherical cavity, which is determined by the method of Wong et al.[24] The ϵ value is taken to be 78.39 throughout the present study to represent an aqueous environment. Because the complexes examined possess positive charges, the dipole moment was evaluated with the procedure of Wong et al. They divided the dipole moment of a charged molecule into two parts, μ_e and μ_N, which correspond to the dipole moment of electrons and that of nuclear charges, respectively. The total dipole moment of the molecule μ is represented by eq 4

$$\mu = \frac{\mu_e(Q + n_e)}{n_e} + \mu_N \tag{4}$$

where Q and n_e are the total charge and the number of electrons, respectively. In the calculation of μ_e, we used the density matrix of the total wave function

$$P^C_{\mu\nu} = C_A^2\, P^A_{\mu\nu} + C_B^2\, P^B_{\mu\nu} + 2C_AC_B\,\det(\mathbf{U})\,\det(\mathbf{V}^+)P_{\mu\nu} \tag{5}$$

where $P_{\mu\nu}$ is the generalized density matrix and where $\mathbf{U}$ and $\mathbf{V}$ are unitary matrices of the corresponding transformation,[25] all of which are defined according to Farazdel et al.[21] $P_{\mu\nu}{}^A$ and $P_{\mu\nu}{}^B$ are usual density matrices of A and B states, respectively. μ_e was calculated from the partial charge on all of the atoms, which is determined so as to reproduce the electrostatic potential evaluated with wave functions at each grid point around the solute molecule.

Computational Details. To calculate the adiabatic states, we used the GAMESS program package[26] with several modifications by us. In all of the calculations, core electrons of Ru (up to 3d) and Os (up to 4f) were replaced with effective core potentials (ECPs), where the (341/321/31) set was used for valence electrons of Ru and the (341/321/21) set was used for those of Os.[27] For C, N, and O, the 6-31G(d) sets were employed, and for H, the 6-31G set was employed. To check the reliability of this basis set system, the electron-transfer matrix element was evaluated with larger basis sets, in which all electron basis sets, [84333/843/75/1][28] augmented with an f-function ($\alpha = 1.235$),[29] 6-311G(d), and 6-31G, were used for Ru, N, C, and H. These two different basis set systems presented almost the same value of the electron-transfer matrix elements.[21,30] Thus, the smaller basis set system was employed throughout the present study.

In **1**, the Ru−NH_3 and Ru−pyrazine bond distances were taken from the X-ray crystal structure,[2] while geometries of NH_3 and pyrazine were optimized by the DFT(B3LYP)[31] method since structural data are not available for these moieties. In the geometry optimization, we used the Gaussian 98 program.[32] In **2**, **3**, and **4**,

(22) (a) To obtain the localized UHF wave functions, we adopted the following strategy. At the beginning, we prepared the localized wave function for the geometry where one of the metal-bridge distances was taken to be very long but where the other was normal. The obtained wave function is well-localized. After a check of S^2 and the spin density, we calculated the wave function of the ions whose metal-bridge distance was taken to be moderately shorter, where we employed the previously calculated, well-localized UHF wave function as an initial guess. Until the metal-bridge distance became the same as that of the real one, we continued this procedure. This technique presented the well-localized, broken-symmetry UHF wave function; for instance, the spin densities on Ru centers of **1** are 1.09 and −0.01, respectively. The bond order analysis showed that the free valence electrons on one metal and those on the other at Δr =0.00 are 0.95 and 0.00 for **1**, 0.92 and 0.02 for **2**, 0.93 and 0.00 for **3**, and 0.91 and 0.00 for **4**. These results indicate that the wave function is well-localized. (b) The S^2 values for the localized UHF wave functions at Δr =0.00 are 0.78 for **1**, 0.80 for **2**, 1.03 for **3**, and 1.04 for **4** (Supporting Information Table S4), indicating that the spin contamination occurs very little in **1** and **2** but occurs somewhat in **3** and **4**. To investigate the nature of the spin contamination of bipyridine systems, we calculated the quartet spin state of the ions because this is considered to contribute considerably to the spin contamination. The unpaired electrons are localized on two metal centers and the bridging ligand in the quartet state. Thus, it is likely that the spin contamination of the quartet spin state would increase the spin density on the bridging ligand and makes the S^2 values somewhat large.

(23) In the present study, UHF wave functions have been used just as basis functions to construct the total wave function, and it might be unsuitable to call it diabatic basis in a precise sense. However, we use the words diabatic or adiabatic throughout the paper to describe the transformation and mixing nature of the wave functions just for convenience.

(24) Wong, M. W.; Frisch, M. J.; Wiberg, K. B. *J. Am. Chem. Soc.* **1991**, *113*, 4776−4782.

(25) King, H. F.; Stanton, R. E.; Kim, H.; Wyatt, R. E.; Parr, R. G. *J. Chem. Phys.* **1967**, *47*, 1936−1941.

(26) Schmidt, M. W.; Baldridge, K. K.; Boatz, J. A.; Elbert, S. T.; Gordon, M. S.; Jensen, J. H.; Koseki, S.; Matsunaga, N.; Nguyen, K. A.; Su, S. J.; Windus, T. L.; Dupuis, M.; Montgomery, J. A. *J. Comput. Chem.* **1993**, *14*, 1347−1363.

(27) Hay, P. J.; Wadt, W. R. *J. Chem. Phys.* **1985**, *82*, 270−283.

(28) Koga, T.; Tatewaki, H.; Matsuyama, H.; Satoh, Y. *Theor. Chem. Acc.* **1999**, *102*, 105−111.

(29) Ehlers, A. W.; Böhme, M.; Dapprich, S.; Gobbi, A.; Höllwarth, A.; Jonas, V.; Köhler, K. F.; Stegmann, R.; Veldkamp, A.; Frenking, G. *Chem. Phys. Lett.* **1993**, *208*, 111−114.

(30) Electron-transfer matrix elements calculated with a smaller basis set and with a larger one are 0.276 and 0.266 eV, respectively.

(31) Becke, A. D. *J. Chem. Phys.* **1993**, *98*, 5648−5652.

(32) Frisch, M. J.; Trucks, G. W.; Schlegel, H. B.; Scuseria, G. E.; Robb, M. A.; Cheeseman, J. R.; Zakrzewski, V. G.; Montgomery, J. A., Jr.; Stratmann, R. E.; Burant, J. C.; Dapprich, S.; Millam, J. M.; Daniels, A. D.; Kudin, K. N.; Strain, M. C.; Farkas, O.; Tomasi, J.; Barone, V.; Cossi, M.; Cammi, R.; Mennucci, B.; Pomelli, C.; Adamo, C.; Clifford, S.; Ochterski, J.; Petersson, G. A.; Ayala, P. Y.; Cui, Q.; Morokuma, K.; Malick, D. K.; Rabuck, A. D.; Raghavachari, K.; Foresman, J. B.; Cioslowski, J.; Ortiz, J. V.; Stefanov, B. B.; Liu, G.; Liashenko, A.; Piskorz, P.; Komaromi, I.; Gomperts, R.; Martin, R. L.; Fox, D. J.; Keith, T.; Al-Laham, M. A.; Peng, C. Y.; Nanayakkara, A.; Gonzalez, C.; Challacombe, M.; Gill, P. M. W.; Johnson, B. G.; Chen, W.; Wong, M. W.; Andres, J. L.; Head-Gordon, M.; Replogle, E. S.; Pople, J. A. *Gaussian 98*, revision A9; Gaussian, Inc.: Pittsburgh, PA, 1998.

Scheme 1

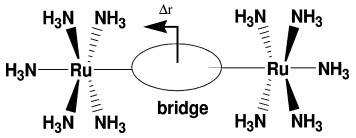

metal−N(ammonia), metal−N(pyrazine), and metal−N(4,4′-bipyridine) distances were taken to be the same as those of **1** because there is no experimental data and because our purpose is to compare them in the same situation.

The energy curves were calculated as a function of the displacement (Δr) of the bridging ligand from the midpoint of the two metal centers (see Scheme 1 for Δr). Along the lines of their procedure, we calculated the diabatic potential energy surface, assuming that the metal−NH_3 distance did not change along the antisymmetric stretching motion of the bridging ligand. This assumption is reasonable because the displacements of metal−NH_3 groups have little influence on the potential energy surface.[33] In **3**, the dihedral angle in 4,4′-bipyridine was fixed to be 40°, which was optimized by changing the dihedral angle by intervals of 10°. This angle is the same as that reported previously.[1] The effect of the dihedral angle on electronic structures will be discussed later.

Results and Discussion

Potential Energy Curve of Diabatic States. As shown in Figure 2, two symmetry-broken wave functions, Ψ_A and Ψ_B, are calculated with the UHF method along the reaction coordinate Δr. These two states are degenerate in the symmetrical structure, $\Delta r = 0$. As shown in Figure 2, single occupied molecular orbitals (SOMOs) of these states are almost localized on each metal center. Here, Ψ_A represents the state in which SOMO is almost localized on the metal of the left-hand side, and Ψ_B represents the other state. These are diabatic states.

The adiabatic states of the ground and excited states are calculated in the gas phase by using eq 2, as shown in Figure 3. In all of these complexes, the adiabatic state exhibits a single minimum for the symmetrical structure ($\Delta r = 0$), indicating that the electronic structures of all of these complexes are delocalized in the gas phase. In Figure 3, we can see the energy splitting between two adiabatic states increases in the order **3** < **4** < **1** < **2**. According to the two-state model, the strength of the mixing depends on the difference in energies ($\Delta H = H_{BB} - H_{AA}$) and the overlap integral (S_{AB}) between two diabatic states; the larger the overlap and the smaller the difference in energy, the larger the mixing becomes. At the seam of crossing between two states, the electron-transfer matrix, V, is discussed in terms of the overlap S_{AB} between two states. The value, V, is calculated by eq 6 using the important parameters, S_{AB}, H_{AB}, H_{AA}, and H_{BB} in eq 2

$$V = (1 - S_{AB}^2)^{-1}[H_{AB} - S_{AB}(H_{AA} + H_{BB})/2] \qquad (6)$$

Actually, V linearly depends on S_{AB}, as shown in Figure 4. Thus, it is worthwhile to clarify the origin of the difference in S_{AB} or the strength of the state mixing in these examined complexes. In the present two-state model, S_{AB} is defined as follows[21]

$$S_{AB} = \langle \Psi_A | \Psi_B \rangle = (\det \mathbf{U})(\det \mathbf{V}^\dagger) \prod_{i=1}^{N} s_{ii} \qquad (7)$$

where **U** and **V** are unitary matrices of the corresponding transformation. Notations used here, except for s_{ii}, are the same as those in ref 21. Here, s_{ii} represents the overlap between corresponding orbitals, $\hat{a}_i$ and $\hat{b}_i$, belonging to each diabatic states.

$$s_{ii} = \langle \hat{b}_i | \hat{a}_i \rangle \qquad (8)$$

We found that all s_{ii} are almost 1.0, except for one overlap term, s_{kk}, between two specific orbitals. Consequently, S_{AB} mainly depends on this overlap, as shown in Figure 4.

$$S_{AB} \propto s_{kk} = \langle \hat{b}_k | \hat{a}_k \rangle \qquad (9)$$

These key orbitals, $\hat{a}_k$ and $\hat{b}_k$, are the corresponding orbitals that are almost the same with canonical β-spin HOMO orbitals in **1**−**4**. The similar relation was previously reported by Koga et al.[34] These $\hat{a}_k$ and $\hat{b}_k$ orbitals are mirror images of each other; one of them is localized on the Ru^1/Os^1 site, and the other is on the Ru^2/Os^2 site. In these orbitals, the d_π orbital expands to the bridge part, as illustrated in Figure 5. Apparently, the overlap integral between $\hat{a}_k$ and $\hat{b}_k$ in **1** and **2** is much larger than that in **3** and **4**; in the latter complexes, these orbitals are completely separated and localized on each metal center.

The s_{kk} term is further divided into six parts, as follows[34]

$$s_{kk} = \sum_{I}^{b,m,ob,m,o} \sum_{J} s_{kk}^{IJ} = \sum_{I}^{b,m,o} s_{kk}^{II} + 2 \sum_{I<J}^{b,m,o} s^{IJ}$$

$$= s_{kk}^{b-b} + s_{kk}^{m-m} + s_{kk}^{o-o} + s_{kk}^{b-m} + s_{kk}^{b-o} + s_{kk}^{m-o} \qquad (10)$$

where b, m, and o stand for bridge ligand, metal center, and remaining part, respectively. In all of the complexes, the m−m, b−m, and b−b pairs provide dominant contributions to s_{kk}, as shown in Figure 6.

The overlap s_{kk}^{m-m} depends on the metal−metal distance; the longer the distance, the less the overlap. In **3** and **4**, the distance is about twice as long as that of **1** and **2**. The longer

(33) To calculate the potential energy surface (PES), we fixed the metal−NH_3 distance and changed only Δr. We examined how much the relaxation of the metal−NH_3 distances influences the PES as follows. We optimized Ru−NH_3 distances with the DFT(B3LYP) method at $\Delta r = 0.00$ and $\Delta r = 0.09$ Å. The maximum difference of the equatorial Ru−NH_3 distance between these two geometries is negligibly small (0.005 Å), as reported.[11] On the other hand, one of the axial Ru−NH_3 distances at $\Delta r = 0.09$ Å becomes longer by 0.0157 Å and another one becomes shorter by 0.0249 Å than those at $\Delta r = 0.00$ Å. To evaluate how much the relaxation of the axial Ru−NH_3 distances influences the PES, we changed the axial Ru−NH_3 distances at $\Delta r =$ 0.09Å, considering the DFT-optimized Ru−NH_3 bond distances (see Supporting Information Figure S1 for details). The adiabatic energy, $E-$, of this geometry is 0.185 eV above the energy at $\Delta r = 0.00$. When the Ru−NH_3 distances are fixed, its energy is 0.175 eV above the energy at $\Delta r = 0.00$. Because these two geometries present almost the same energy, it is likely that the relaxation of the Ru−NH_3 distance influences the PES very little. For **4**, we also examined the influence of the relaxation of the metal−H_3 distances for the PES (see Supporting Information Figure S2 for details).

(34) Koga, N.; Sameshima, K.; Morokuma, K. *J. Phys. Chem.* **1993**, *97*, 13117−13125.

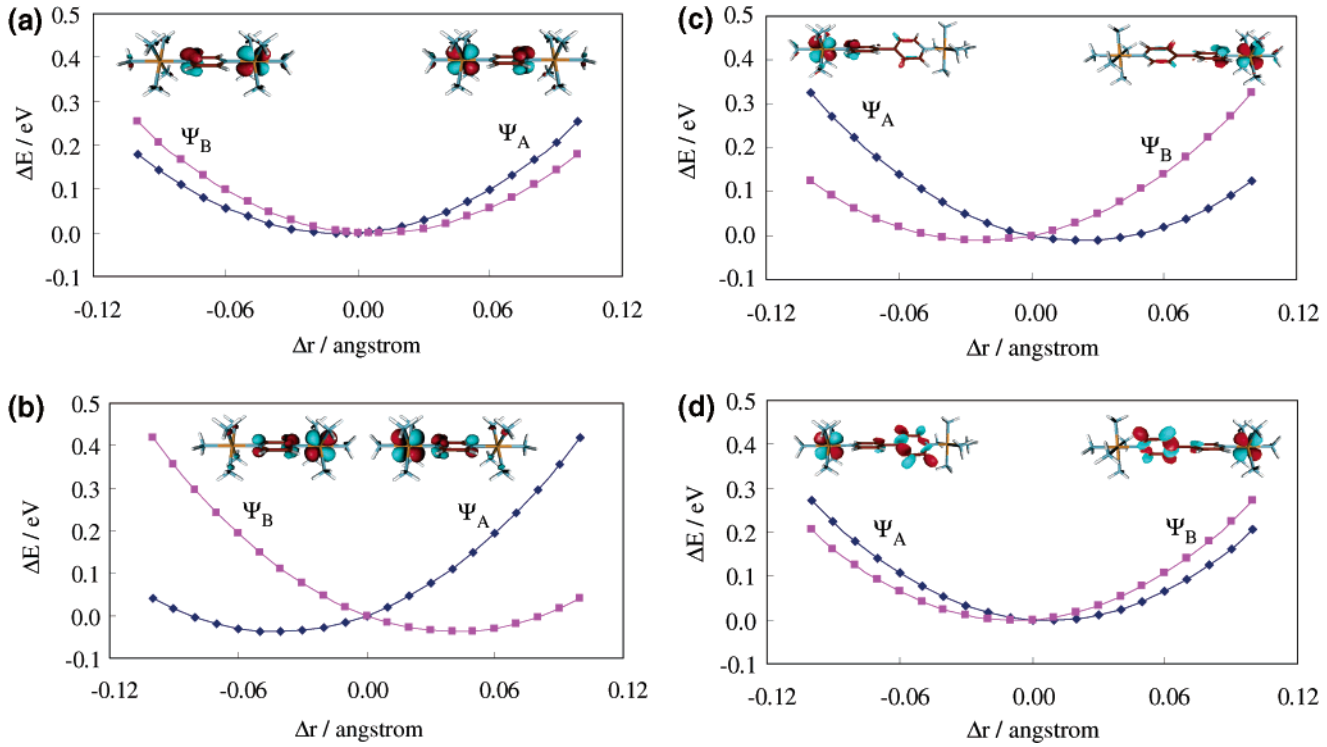

Figure 2. Energy curves and SOMOs of two symmetry-broken wave functions, Ψ_A and Ψ_B; (a) $[(NH_3)_5Ru-pyrazine-Ru(NH_3)_5]^{5+}$ (**1**), (b) $[(NH_3)_5Os-pyrazine-Os(NH_3)_5]^{5+}$ (**2**), (c) $[(NH_3)_5Ru(4,4'\text{-bipyridine})Ru(NH_3)_5]^{5+}$ (**3**), and (d) $[(NH_3)_5Os(4,4'\text{-bipyridine})Os(NH_3)_5]^{5+}$ (**4**).

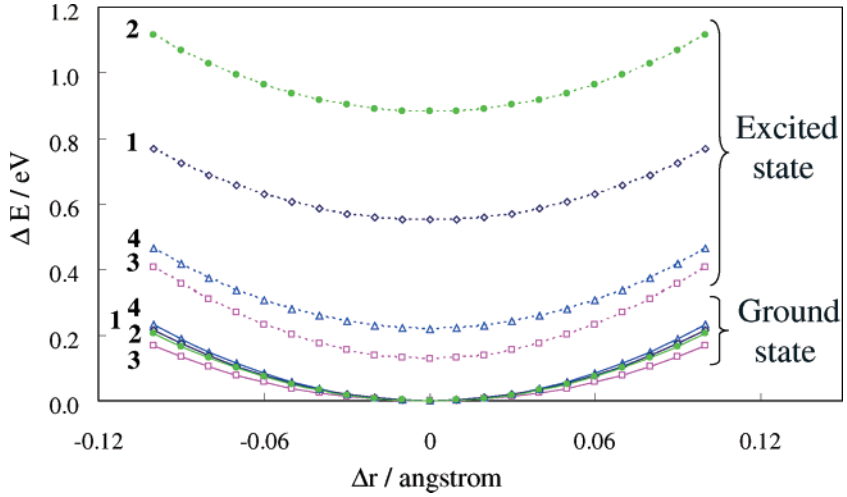

Figure 3. Energy curves of diabatic states. Solid and dotted lines represent the energy curves of the ground state and the excited state, respectively; ◇ $[(NH_3)_5Ru-pyrazine-Ru(NH_3)_5]^{5+}$ (**1**), ● $[(NH_3)_5Os-pyrazine-Os(NH_3)_5]^{5+}$ (**2**), □ $[(NH_3)_5Ru(4,4'\text{-bipyridine})Ru(NH_3)_5]^{5+}$ (**3**), and △ $[(NH_3)_5Os(4,4'\text{-bipyridine})Os(NH_3)_5]^{5+}$ (**4**).

metal−metal distance in **3** and **4** leads to the significantly smaller s_{kk}^{m-m} than that of **1** and **2**. The overlap s_{kk}^{b-m} between the metal part and the bridge part is mainly determined by the overlap between the metal d_π orbital in $\hat{b}_k$ ($\hat{a}_k$) and the π and π^* orbitals of the bridging ligand in $\hat{a}_k$ ($\hat{b}_k$). Since the d_π orbital of Os spatially expands more than that of Ru,[35] the overlaps between the Os d_π orbital and the π^* orbital on the bridge ligands of **2** and **4** are larger than those of **1** and **3**. The overlap between the 4,4′-bipyridine π^* orbital of $\hat{b}_k$ ($\hat{a}_k$) and the metal d_π orbital of $\hat{a}_k$ ($\hat{b}_k$) in **3** and **4** is much smaller than the overlap between the pyrazine π^* and the metal d_π orbitals in **1** and **2**, as is easily seen in Figure 5c,d. Therefore the order of s_{kk}^{b-m} is **3** < **4** < **1** < **2**.

Interestingly, a remarkable difference in s_{kk}^{b-b} is observed among these complexes, whereas the shapes of the orbitals are very similar to each other. It is likely that, because the Os d_π orbital is closer in energy to the pyrazine π^* orbital than the Ru d_π orbital is, the π^* orbital contributes more to the diabatic state in the Os complex than it does in the Ru complex.[36] The contribution of the π^* orbital to $\hat{a}_k$ and $\hat{b}_k$ was evaluated by the following equation

$$\phi = C_\pi \phi_\pi + C_{\pi^*} \phi_{\pi^*} \tag{11}$$

(35) Fraga, S.; Saxena, K.; Karwowski, J. *Handbook of Atomic Data*; Elsevier: Amsterdam, The Netherlands, New York, 1976.

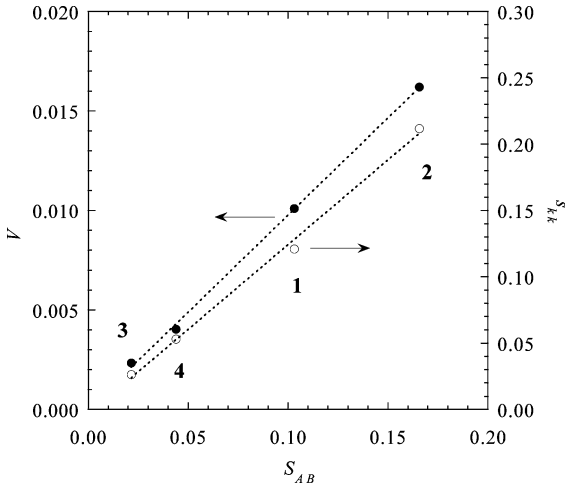

Figure 4. Correlation (○) between electron-transfer matrix, V, and S_{AB} and correlation (●) between s_{kk} and S_{AB}. Dotted lines are determined by the least-squares method.

where ϕ is the contribution of the bridge moiety to the corresponding orbital $\hat{a}_k$ ($\hat{b}_k$). The ϕ_π and ϕ_{π^*} are canonical orbitals of 4,4′-bipyridine calculated by the HF method. The values of $C^2_{\pi^*}$ of **3** and **4** are 0.006 and 0.018, respectively. This difference leads to the difference in s^{b-b}_{kk} between **3** and **4**. In **1** and **2**, the $\hat{a}_k$ and $\hat{b}_k$ orbitals exhibit amplitude, to some extent, on the bridge group, as shown in Figure 5a,b, which leads to the larger s^{b-b}_{kk} value of **2** than that of **1**.

Summarizing the above discussion, the overlaps s^{m-m}_{kk}, s^{b-m}_{kk}, and s^{b-b}_{kk} ($\propto S_{AB}$) increase in the order Ru < Os and in the order **3** and **4** < **1** and **2**. Thus, the energy splitting between two diabatic states increases in the order **3** < **4** < **1** < **2**. These differences in overlap, S_{AB}, are key factors for localized versus delocalized electronic structure in aqueous solution, as will be discussed in the next section.

In Aqueous Solution. Free energy curves (FEC) in aqueous solution are shown in Figure 7. In **1** and **2**, FEC possesses a single minimum for the symmetric geometry ($\Delta r = 0$), as is the case for those in the gas phase. The FEC of **3** has two minima at $\Delta r = \pm 0.08$Å, showing that the electronic structure of **3** is localized in aqueous solution. The key to understand the difference in **3** from the others is the dipole moment, which is computed by eq 4. The dipole moment is zero at the point of $\Delta r = 0$ in all of the complexes due to the symmetry of the total wave function. It increases with an increase in Δr. Apparently, the dipole moment change is much larger in **3** than it is in the others, as shown in Figure 8. In **4**, FEC is influenced by the dihedral angle (δ) between two pyridyl rings. When δ is 40°, its electronic structure is delocalized, as shown in Figure 9. However, it becomes localized when δ is 80°. Because of the energy difference between the minima at $\delta = 40$ and 80°, the electronic structure of **4** is between the localized and delocalized one (class II). The effect of the dihedral angle will be discussed in more detail later.

(36) To compare the orbital energy of Os with that of Ru, we calculated $[M(NH_3)_5]^{2+}$ (M = Ru or Os) with the HF method. The orbital energies of the d_π orbital are −0.6908 eV for Ru and −0.6231 eV for Os.

Oh et al. studied how much the dipole moment of diruthenium complexes changes upon going to the excited state from the ground state in water using electronic absorption (Stark effect) spectroscopy.[9] They reported that the change is about 0 (D) for **1** and 29 (D) for **3**. As is clearly shown in Figure 7, the electronic structure of **1** is delocalized at the ground state in aqueous solution. In the electronic absorption spectrum, the transition should be from the delocalized electronic structure at the ground state to the delocalized structure at the excited state. On the other hand, the electronic structure of **3** is localized at the equilibrium geometry at the ground state in aqueous solution ($\Delta r = 0.08$Å). The dipole moment was evaluated to be −17 and 20 (D) at the ground and excited states, respectively. The calculated change of the dipole moment is about 37 (D). These computational results of the dipole moment change are consistent with the experimental data.

Change of the dipole moment is induced by the mixing ratio of two diabatic states (see eq 5) whose dipole moment directions are opposite to each other, as illustrated in Figure 8. In the present two-state model, the mixing ratio R depends on H_{AB}, ΔH, and S_{AB}, as represented by eq 12

$$R = \frac{C_B - C_A}{C_B + C_A} = \sqrt{\frac{1 + S_{AB}}{1 - S_{AB}}} \tan\theta \qquad (12)$$

where θ is given by solving eq 2

$$\theta = \frac{1}{2}\tan^{-1}\left\{\frac{\sqrt{1 - S^2_{AB}}}{2}\frac{\Delta H}{H_{AB} - S_{AB}\left(\frac{H_{AA} + H_{BB}}{2}\right)}\right\} \qquad (13)$$

When $\Delta r = 0$, two diabatic states are in the same energy ($\Delta H = 0$), which leads to $R = 0$; this means that the two states mix in the same ratio ($C_A = C_B$). In this case, the dipole moment is 0. At $\Delta r \neq 0$, on the other hand, the mixing ratio is not equivalent, and the dipole moment is induced. As R increases, the localization of the adiabatic wave function increases. Figure 10 shows the change of R as a function of Δr. For $\Delta r > 0$, the sign of R is positive for **1** and **2** and is negative for **3** and **4**. This sign shows which state, Ψ_A or Ψ_B, is dominant at $\Delta r > 0$. In **1** and **2**, Ψ_B is dominant in the adiabatic states, as shown in Figure 2a,b. On the other hand, Ψ_A is dominant in the adiabatic states of **3** and **4**. One can see that the change of R of **3** is much larger than that of the others, which means the contribution of one diabatic state considerably increases with increase in Δr; in other words, the adiabatic wave function tends to localize on one center in **3** to a greater extent than it does in the others.

Because tan and $\tan^{-1}$ are monotonous functions and because S_{AB} is very small, the mixing ratios, R, can be compared with each other using the following quantity, R'

$$R' = \frac{\Delta H}{H_{AB} - S_{AB}\left(\frac{H_{AA} + H_{BB}}{2}\right)} \qquad (14)$$

The larger R' is, the more localized the electronic structure is. As represented by eq 13, the mixing ratio is determined

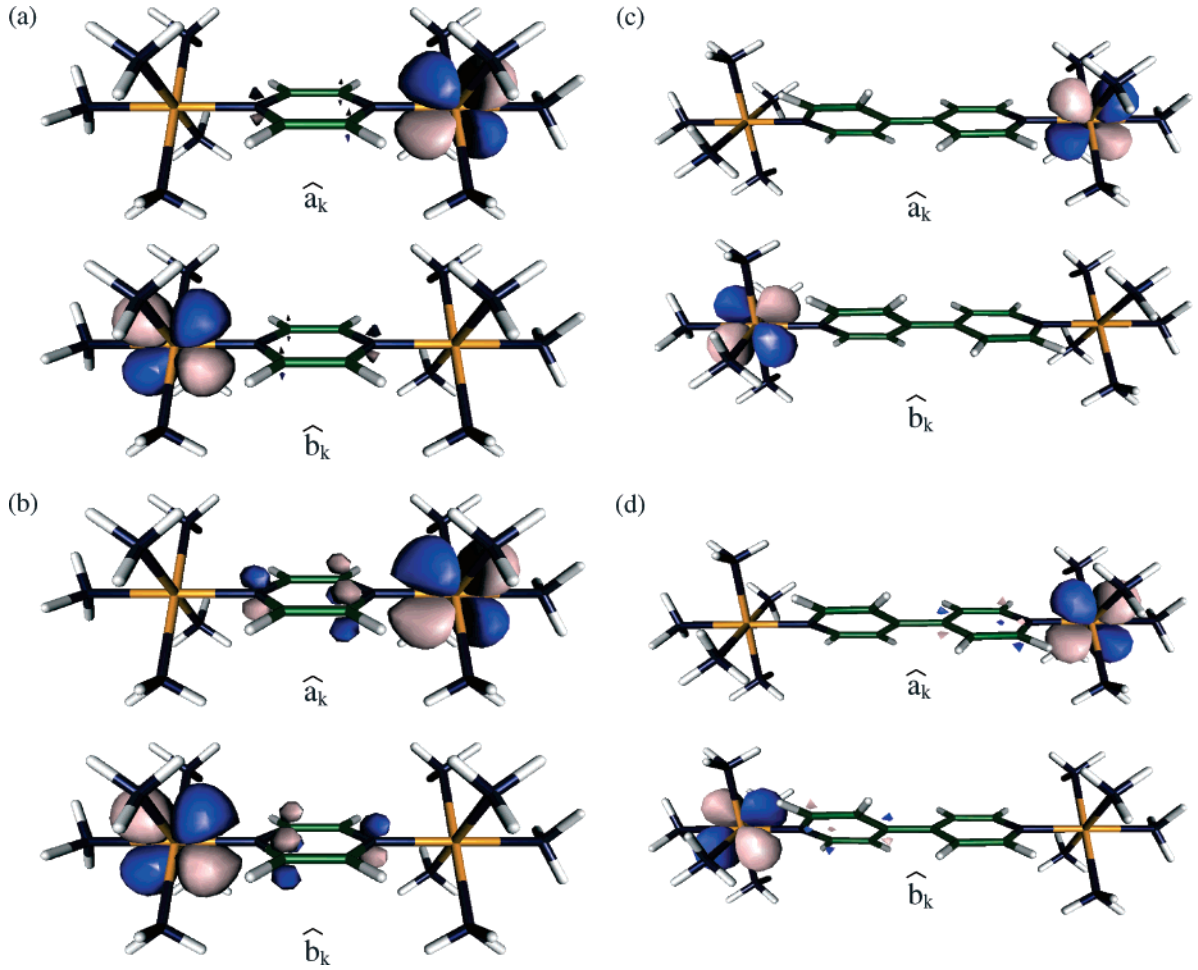

Figure 5. Corresponding orbitals $\hat{a}_k$ and $\hat{b}_k$, which are almost the same as the canonical β-spin HOMO orbitals; (a) $[(NH_3)_5Ru-pyrazine-Ru(NH_3)_5]^{5+}$ (**1**), (b) $[(NH_3)_5Os-pyrazine-Os(NH_3)_5]^{5+}$ (**2**), (c) $[(NH_3)_5Ru(4,4'\text{-bipyridine})Ru(NH_3)_5]^{5+}$ (**3**), and (d) $[(NH_3)_5Os(4,4'\text{-bipyridine})Os(NH_3)_5]^{5+}$ (**4**).

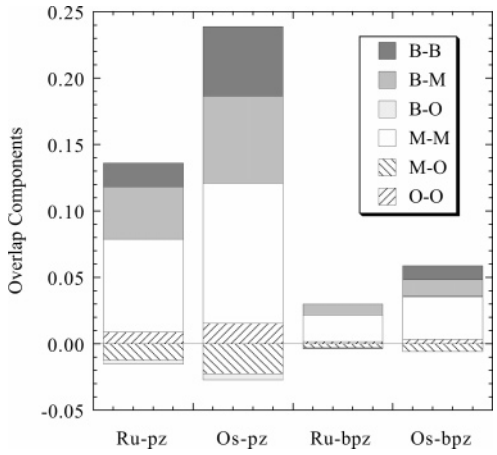

Figure 6. Overlap components, s_{kk}^{b-b}, s_{kk}^{b-m}, s_{kk}^{b-o}, s_{kk}^{m-m}, s_{kk}^{m-o}, and s_{kk}^{o-o}, of $[(NH_3)_5Ru-pyrazine-Ru(NH_3)_5]^{5+}$ (**1**), $[(NH_3)_5Os-pyrazine-Os(NH_3)_5]^{5+}$ (**2**), $[(NH_3)_5Ru(4,4'\text{-bipyridine})Ru(NH_3)_5]^{5+}$ (**3**), and $[(NH_3)_5Os(4,4'\text{-bipyridine})Os(NH_3)_5]^{5+}$ (**4**). The b, m, and o represent the bridge part, the metal center, and the other part.

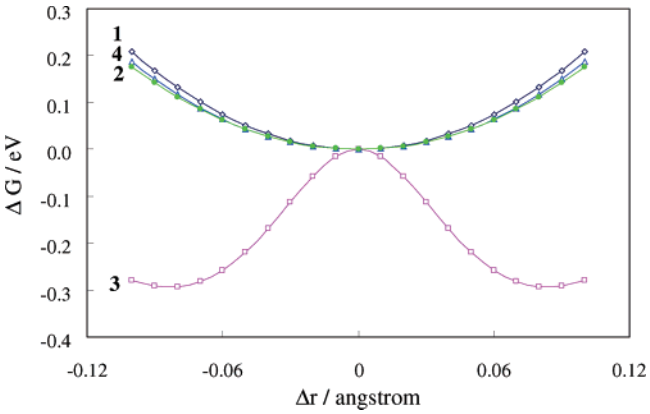

Figure 7. Free energy curves of **1**, **2**, **3**, and **4** in aqueous solution; ◇ $[(NH_3)_5Ru-pyrazine-Ru(NH_3)_5]^{5+}$ (**1**), ● $[(NH_3)_5Os-pyrazine-Os(NH_3)_5]^{5+}$ (**2**), □ $[(NH_3)_5Ru(4,4'\text{-bipyridine})Ru(NH_3)_5]^{5+}$ (**3**), and △ $[(NH_3)_5Os(4,4'\text{-bipyridine})Os(NH_3)_5]^{5+}$ (**4**).

by a subtle balance among several parameters such as S_{AB}, H_{AB}, etc. It should be emphasized that the solvation energy, which is mainly determined by the dipole moment of the complex, increases enough to stabilize the localized electronic structure when the two coefficients, C_A and C_B, are remarkably different. In **3**, R' is much larger than it is in the others because ΔH is the largest and S_{AB} is the smallest, as discussed above. This leads to the much larger dipole moment in **3** than in the others, which further leads to the larger stabilization energy by polar solvent. Thus, the electronic structure of **3** is localized in aqueous solution.

FEC along Rotation of the Bridge Group. In **3** and **4**, two pyridyl rings can rotate around the C−N and/or the N−N

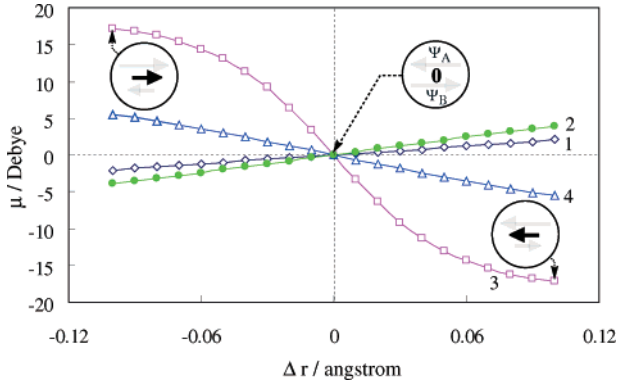

Figure 8. Changes of the dipole moment along Δr. In the solid circle, the dipole moments of diabatic states at $\Delta r = -0.10$, 0.0, and +0.10 are schematically shown; ◇ $[(NH_3)_5Ru-pyrazine-Ru(NH_3)_5]^{5+}$ (**1**), ● $[(NH_3)_5Os-pyrazine-Os(NH_3)_5]^{5+}$ (**2**), □ $[(NH_3)_5Ru(4,4'\text{-bipyridine})Ru(NH_3)_5]^{5+}$ (**3**), and △ $[(NH_3)_5Os(4,4'\text{-bipyridine})Os(NH_3)_5]^{5+}$ (**4**).

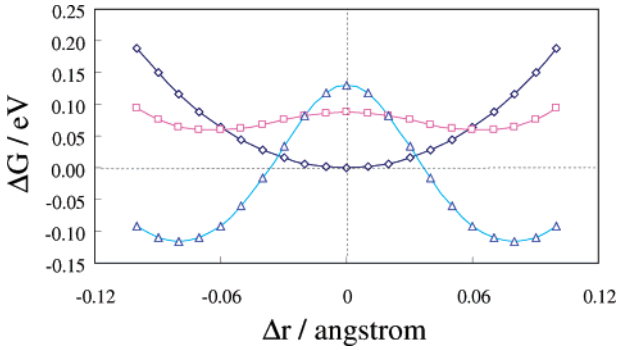

Figure 9. Free energy curves of $[(NH_3)_5Os(4,4'\text{-bipyridine})Os(NH_3)_5]^{5+}$ (**4**) at $\delta = 40$ (◇), 70 (□), and 80° (△). The standard of the free energy is that at 40° and $\Delta r = 0$. The δ is the dihedral angle between two pyridyl planes of 4,4′-bipyridine.

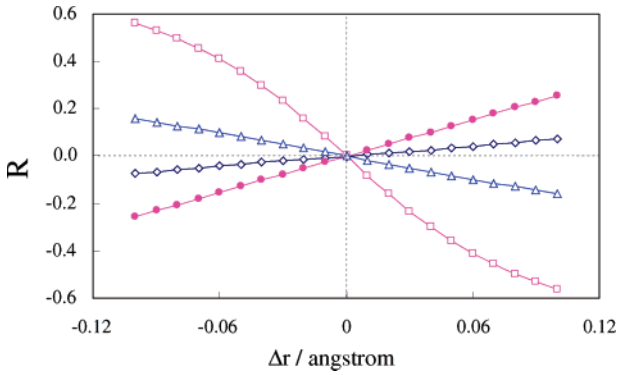

Figure 10. Mixing ratio R versus Δr; ◇ $[(NH_3)_5Ru-pyrazine-Ru(NH_3)_5]^{5+}$, ● $[(NH_3)_5Os-pyrazine-Os(NH_3)_5]^{5+}$, □ $[(NH_3)_5Ru(4,4'\text{-bipyridine})Ru(NH_3)_5]^{5+}$, and △ $[(NH_3)_5Os(4,4'\text{-bipyridine})Os(NH_3)_5]^{5+}$.

bond axis. The increase in the dihedral angle (δ) decreases the overlap between the p_π orbital of C_4 and C_4', which further changes the energy levels of the π and π^* orbitals of the bridge group, and therefore, the electronic structure of these complexes is influenced by this rotation. It is interesting to investigate how much the localization/delocalization of the electronic structure depends on the rotation.

The FEC of **4** were evaluated at $\delta = 40$, 70, and 80°, as shown in Figure 9. Although the electronic structure of **4** is delocalized at $\delta = 40°$, as was discussed previously, it is sufficiently localized at 80°. As previously mentioned, the dipole moment, which has great influence on the localization in aqueous solution, is mainly determined by the parameter R' (eq 14). Because the change of the dihedral angle between two pyridyl planes has little influence on the $d_\pi-\pi^*$ interaction, ΔH is almost constant. From eq 14, we can say that the difference in FEC among $\delta = 40$, 70, and 80° is mainly governed by the overlap S_{AB} and H_{AB}. Because H_{AB} is almost proportional to S_{AB}, S_{AB} is the main factor that determines the localization/delocalization of these complexes. S_{AB} decreases with an increase in the dihedral angle; for instance, S_{AB} is 0.044 at $\delta = 40°$ ($\Delta r = 0$) but significantly decreases to 0.01 at $\delta = 80°$ ($\Delta r = 0$). This small S_{AB} at $\delta = 80°$ induces the large dipole moment at $\Delta r \neq 0$, which leads to the localized electronic structure at this angle.[37]

Conclusions

We have theoretically studied the electronic structures of the Creutz−Taube complex and its analogues. They have attracted a great deal of interest into understanding their electronic structure, namely, localization or delocalization. There are two important requirements to understand the electronic structure of the system. One is a multiconfigurational description in the wave functions, which is caused by an inherent character of the mixed-valence metal complex, and the other is solvation effect, which is not negligible. In the present study, we have theoretically investigated these complexes by consideration of a two-state model based on ab initio molecular orbital theory and the dielectric continuum model, and we related the localization/delocalization of the electronic structure with fundamental parameters, such as overlap and energy gaps. Although the calculation is not sufficient for the understanding of the true nature of the ions, our work showed the important factors which determine the localization/delocalization.

It is found that all of the electronic structures of the examined complexes would be delocalized in the gas phase, but the electronic structure of **3** with a long bridge, $[(NH_3)_5Ru(4,4'\text{-bipyridine})Ru(NH_3)_5]^{5+}$, shows a localized electronic structure in an aqueous environment. In **4**, the electronic structure changes as the dihedral angle becomes large. The localized electronic structures of the complexes are interpreted in terms of the magnitude of the mixing of two diabatic states, which is small; because of a large ΔH and a small S_{AB}, the mixing ratio R is much larger. Thus, one of two states becomes dominant enough, and the dipole moment of the complex significantly increases, which leads to large solvation effects. In the other two complexes, **1** and **2**, π and π^* orbitals in pyrazine and bipyridine interact well with the d_π orbital of the metal center. As a result, the overlap S_{AB} becomes sufficiently large to induce the electron delocalization. In **4**, we wish to propose the possibility that the electronic structure can be designed by introducing some substituents at the C_3 and C_3' positions of 4,4′-bipyridine; such substituents increase the dihedral angle between two pyridyl plane to decrease S_{AB}.

(37) This decrease arises from the decrease in s_{kk}^{b-b}, as shown in Figure 6.

Acknowledgment. This work was financially supported by Grant-in-Aids on basic research (No. 15350012), Priority Areas for "Reaction Control of Dynamic Complexes" (No. 420) and "Molecular Theory for Real Systems" (No. 461), Creative Scientific Research, and NAREGI project from the Ministry of Education, Science, Sports, and Culture. D.Y. thanks the Grant-in Aid for JSPS Fellows. Some theoretical calculations were performed with SGI workstations of the Institute for Molecular Science (Okazaki, Japan), and some of them were carried out with PC cluster computers in our laboratory.

Supporting Information Available: Potential energy surface and geometries of **1**. This material is available free of charge via the Internet at http://pubs.acs.org.

IC060173A